UCRL-ID-143900

# HULLAC-based Simulations of Non-LTE Emission Spectra

*K. B. Fournier*

**April 12, 2001**

***U.S. Department of Energy***

Lawrence
Livermore
National
Laboratory

Approved for public release; further dissemination unlimited

## DISCLAIMER

This document was prepared as an account of work sponsored by an agency of the United States Government. Neither the United States Government nor the University of California nor any of their employees, makes any warranty, express or implied, or assumes any legal liability or responsibility for the accuracy, completeness, or usefulness of any information, apparatus, product, or process disclosed, or represents that its use would not infringe privately owned rights. Reference herein to any specific commercial product, process, or service by trade name, trademark, manufacturer, or otherwise, does not necessarily constitute or imply its endorsement, recommendation, or favoring by the United States Government or the University of California. The views and opinions of authors expressed herein do not necessarily state or reflect those of the United States Government or the University of California, and shall not be used for advertising or product endorsement purposes.

This work was performed under the auspices of the U. S. Department of Energy by the University of California, Lawrence Livermore National Laboratory under Contract No. W-7405-Eng-48.

This report has been reproduced directly from the best available copy.

Available electronically at http://www.doc.gov/bridge

Available for a processing fee to U.S. Department of Energy
And its contractors in paper from
U.S. Department of Energy
Office of Scientific and Technical Information
P.O. Box 62
Oak Ridge, TN 37831-0062
Telephone: (865) 576-8401
Facsimile: (865) 576-5728
E-mail: reports@adonis.osti.gov

Available for the sale to the public from
U.S. Department of Commerce
National Technical Information Service
5285 Port Royal Road
Springfield, VA 22161
Telephone: (800) 553-6847
Facsimile: (703) 605-6900
E-mail: orders@ntis.fedworld.gov
Online ordering: http://www.ntis.gov/ordering.htm

OR

Lawrence Livermore National Laboratory
Technical Information Department's Digital Library
http://www.llnl.gov/tid/Library.html

# HULLAC-based simulations of non-LTE emission spectra

Kevin B. Fournier
*Physics and Advanced Technology, Lawrence Livermore National Laboratory*
P. O. Box 808, L-41, Livermore, CA 94551 USA
fournier2@llnl.gov

April 12, 2001

**Abstract**

This document describes the calculations I have carried out to synthesize spectra for test cases Ar1, Ge1, Ba1 and Au1. First, a brief description of how HULLAC generates atomic data is presented. Next, the implementation of those data in a collisional-radiative (CR) model is described. Two approaches are taken: First, the HULLAC data are entered into the CR rate matrix, and the relative populations of each ion charge state as given by an off-line Monte Carlo calculation are used to constrain the resulting level populations. Alternatively, the HULLAC data-filled CR rate matrix is inverted with out constraining the relative ion populations; the resulting average ion charge $< Z >$ is significantly different between the two calculations. My resulting b-b, b-f and f-f emission spectra are presented in figures. This work was performed under the auspices of the U.S. Department of Energy by University of California Lawrence Livermore National Laboratory under contract No. W-7405-Eng-48.

# 1 INTRODUCTION

Emission spectra from non-local thermodynamic equilibrium (non-LTE) plasmas are used to probe density and temperature conditions and equilibrium configurations in the plasma. All simulations of the spectra and their coupling to the plasma environment are undergirded by calculations of atomic data. Therefore, tests of simulation codes are necessary for confidence in our understanding of non-LTE plasmas. In particular, the atomic data constituents of the spectral models, and the spectral simulation (including calculation of the charge state distribution) can be decoupled and tested independently. However, for the present code comparisons, the integrated problem of calculating non-LTE emission spectra from theoretical atomic data is being addressed for a collection of increasingly sophisticated problems.

I have performed line-by-line, or detailed, calculations for the Ar1, Ge1, Ba1 and Au1 test cases using the HULLAC atomic physics package. For the K-shell argon test case, this is probably quite adequate; for the more complicated L- and M-shell test cases, limitations on the size of the models means that the detailed treatment probably misses many spectral features. For example, in the Zn-like ion, one can compute the emissivity for the two $3d^9(4s^2)5f\ J{=}1{\rightarrow}3d^{10}(4s^2)\ J{=}0$ X-ray transitions that give rise to distinct lines. At the lowest densities, these two lines are all that need to be considered for the Zn-like X-ray spectrum. However, the two $4s^2$ electrons can be distributed into nine other configurations ($4s4p$, $4s4d$, $4p^2$, $\cdots$), and for each $4\ell4\ell'$ pair of occupied orbitals, the totality of transitions for each $3d^9(4\ell4\ell')5f\ J' \rightarrow 3d^{10}(4\ell4\ell')\ J$ array makes up a distinct transition array [1]. I have neglected all of these more-highly-excited transition arrays in the Ba1 M-shell test case, and have attempted to include some of them in the Au1 M-shell test case. The totality of the transition arrays identified above comprises a super transition array (STA) [2]. Clearly, a treatment of the STAs in several ions is necessary to simulate the complicated M-shell spectra of the present work. Formulae to compute the relative strengths of STAs in the spectra of some ion (or collection of ions) require assumptions about the population of ionic super-configurations that are only correct in local thermodynamic equilibrium (LTE). The departure of an ionic system from LTE, as obtains for the present test cases, puts us in a regime where the STA formalism is not rigorously appropriate, and where detailed treatments are overwhelmed by complexity; the comparison of many calculations for these test cases will be an illuminating exercise. In what follows, the original citations for the physics incorporated in the HULLAC package and for the collisional-radiative (CR) techniques that I employ are given. Interspersed with those citations, references are also given to recent experiments that I have been involved in, which test atomic data issues specific to HULLAC's capabilities. The citations of relevant experimental work are by no stretch of the imagination complete or even fair to other experimental groups that rely on HULLAC's capabilities. Details of my approach to the different test cases are given in Section 3, and a brief description of my calculation of bound-free and free-free emission spectra is given in Section 4.

# 2 HULLAC

## 2.1 Atomic Structure

The atomic data used to generate the spectra of the present work were generated with the Hebrew University Lawrence Livermore Atomic Codes (HULLAC). The atomic structure part of the HULLAC package includes the graphical angular momentum coupling code ANGLAR [3] and the fully relativistic parametric potential code RELAC of Klapisch *et al.* [4, 5, 6]. ANGLAR uses the graphical angular recoupling program NJGRAF [3] to generate fine structure levels in a $jj$-coupling scheme for a set of user-specified electron configurations. The art of running HULLAC lies in selecting the configurations to be included in a model. RELAC divides the Dirac Hamiltonian into a spherical, zero$^{th}$ order contribution and a perturbation:

$$H_D{\approx}H_0 + H_1 + higher\ \ order\ \ terms. \tag{1}$$

The zero$^{th}$ order Hamiltonian is made up of the sum over all $N$ electrons of the Dirac kinetic energy, the electron-nuclear interaction and the interaction between an electron and a spherically averaged potential arising from all other electrons:

$$H_0 = \sum_i^N \left[ h_i^D + \frac{Z}{r_i} + V(r_i) \right]. \tag{2}$$

The perturbation now includes only the difference between the exact electrostatic interaction and the interaction between the electrons and the spherically averaged potential:

$$H_1 = \left[ \sum_{i<j}^N \frac{1}{r_{ij}} - V(r_i) \right]. \tag{3}$$

For a given ion, RELAC solves the Dirac equation by varying an analytic ionic potential [6] in order to minimize the average energy of a configuration (or a set of configurations). The potential has the form:

$$V(\alpha, r) = -\frac{1}{r_{ij}} \left( \sum_{s=1}^N q_s f(l_s, \alpha_s, r) + I \right) \tag{4}$$

where $q_s$ is the number of electrons in each shell, the sum over $s$ runs over the $N$ occupied shells of the ion, $l_s$ is the orbital quantum number of a shell and $I$ is the degree of ionization plus 1. The function $f$ is given by:

$$f(l_s, \alpha_s, r) = e^{-\alpha_s r} \sum_{k=0}^{2l_s+1} \left( 1 - \frac{k}{2l_s+2} \right) \frac{(\alpha_s r)^k}{k!}. \tag{5}$$

The function $V(\alpha, r)$ represents the potential due to the superposition of a point nuclear charge, $+Z$,

$$\frac{Z\delta(r)}{4\pi r^2} = \left( \sum_{s=1}^N q_s + I \right) \frac{\delta(r)}{4\pi r^2}$$

and a radial electron charge density of the form:

$$\frac{1}{4\pi r^2}\rho(r) = -\sum_{s=1}^N q_s A(\alpha_s, l_s) \left( r^{l_s+1} e^{-\frac{\alpha_s r}{2}} \right)^2.$$

In the above equation $A(\alpha_s, l_s)$ is a normalizing factor, and the last quantity is the nodeless Slater-type wavefunction. The free parameters $\alpha_s$ are proportional to the inverse of the mean radius of a shell. Orthogonality of the wavefunctions is insured by the use of one potential for all electrons; the need for overlap integrals and recoupling coefficients is avoided. Once the zero$^{th}$ order wavefunctions which minimize the configuration-average energy of each configuration (or set of configurations) have been found, RELAC calculates the multiconfiguration, intermediate-coupling energy eigenvalues of the fine structure levels.

The physical state of some ionic energy level can contain contributions from many components of a pure basis representation. The Coulomb operator is a two-electron operator, and hence, can have nonvanishing elements when evaluated between configurations that differ by one or two electron orbitals. It is thus that the energy calculation for the levels of a given configuration can be perturbed by "mixing" (or configuration interaction - CI) with levels of a different configuration. The calculation of the CI contribution to a level's energy depends on an infinite number of contributions from all states with the same parity and total $J$-value, including states in the continuum. The more widely separated in energy two levels are, the weaker the interaction between them will be. CI effects on the level structure giving rise to X-ray spectra in highly charged, high-Z ions are mainly due to "accidental"

level crossings [7]. Consequences of the multiple basis components in the physical states of energy levels, which are manifested in CR emissivities, are perturbations of energy eigenvalues and redistribution of transition oscillator strengths [7, 8]. Another consequence of CI is an enabling of what would be "forbidden" transitions corresponding to two electron jumps [9, 10]; this, in fact, can quench classes of transitions [11]. The effect of CI on transition arrays can be more pronounced than in the cases of individual transitions between well separated levels [12, 13]. For all the cases in the present work, the above CI effects are included in the structure calculations.

Higher order energy terms, including the Breit interaction energy, vacuum polarization [14] and electron self energy corrections [15, 16, 17], are then added to a level's energy. The latter two terms make up the Lamb shift to the electron's energy, and affect mainly the orbitals which penetrate the nucleus ($ns_{1/2}$ and $np_{1/2}$ in $jj$-notation). RELAC finds these contributions according to

$$\Delta E_{nlj} = \frac{\left(Z^{\text{eff}}_{nlj}\alpha\right)^4}{\pi\alpha n^3} F\left(Z^{\text{eff}}_{nlj}\alpha\right) \tag{6}$$

where $Z^{\text{eff}}_{nlj}$ is an effective screened nuclear charge and $\alpha$ is the fine structure constant. The function $F\left(Z^{\text{eff}}_{nlj}\alpha\right)$ [15, 16, 17] reflects the departures from hydrogenic atomic structure in the multielectron ion under consideration. The effective $Z$ for a given orbital maps RELAC's wavefunctions onto the tabulations of hydrogenic electron orbital self energies by Mohr [15, 16, 17] and is found (for $s$ and $p$ orbitals) by requiring that the expectation value of the orbital radius computed above, $\langle r_{nlj}\rangle$ equals the corresponding screened hydrogenic value with the same Dirac energy [6]. Higher angular momentum orbitals, $l > p$, are treated with the approximations of Erickson [18]. RELAC assumes the nuclear charge to be a point charge, $\rho = Z\delta(r)$; a finite charge distribution $\rho = \rho(r)$ for the nuclear charge would have an effect less than or equal in magnitude to the effect of the above higher order energy terms only for orbitals which penetrate the nucleus ($1s_{1/2}$, $2s_{1/2}$, etc.).

## 2.2 Transition Rates

Radiative transition rates are then computed for any multipole operator requested according to the formalism in Ref. [19]. The transition rate calculation by RELAC is carried out in the Coulomb gauge (thus, in the dipole velocity form of the transition operator matrix element [19]) and explicitly includes retardation effects [20]. The radiative transition rate and the dipole oscillator strength in atomic units (for E1 transitions) are related by:

$$(2j_l + 1)f_{l\to u} = (2j_u + 1)\frac{A_{u\to l}}{2\alpha^3\sigma^2} \tag{7}$$

where $\sigma$ is the transition energy. RELAC's full multiconfiguration wavefunctions are used to compute the radiative transition rates; thus, configuration mixing affects the calculated oscillator strengths. For the present spectral calculations, only E1 and electric quadrupole (E2) transitions are considered. In the absence of a radiation field, only radiative decays (and not bound-bound absorption) are considered in the calculations of synthetic spectra described below.

Our spectral calculations include autoionization decays from excited levels in the continuum to all accessible levels in the next ion state; observations of a case where the autoionization rates dramatically affect the branching ratio for radiative decays of X-ray lines in neonlike ions is seen in Ref. [7]. The autoionization rates are found by evaluating the two-electron Coulomb interaction operator between multiconfiguration states of the ion with charge $Z$ and the ion with charge $(Z+1)$ and a free, outgoing electron [21]

$$A^A_{jf} = \sum_{\tilde{j}} \sum_{J_T, M_T} \left| \langle \Psi_f(\Gamma, J)\tilde{j} J_T M_T | \left[ \sum_{ij(i<j)} \frac{1}{r_{ij}} \right] | \Psi_\beta(\Gamma'', J''_T, M''_T)\rangle \right|^2 \tag{8}$$

where the state $|\Psi_\beta\rangle$ is the multiconfiguration wavefunction of the initial ion state, $|\Psi_f\rangle$ is the final state in the next ion and $\tilde{j} = (E_{\tilde{j}}, l_{\tilde{j}}, \tilde{j})$ is a free electron wavefunction. The outermost sum in equation 8 is over the continuum orbitals making up the partial waves of the outgoing free electron. RELAC uses the factorization technique of Bar-Shalom, Klapisch and Oreg [22] in equation 8 in order to split the matrix element into an angular part depending only on the bound electrons and an interpolation scheme to compute the radial integrals very quickly on a grid of free electron energies. Details of the procedure, and a derivation of the factored form of the transition operator can be found in Ref. [21]. In the present calculations, the contribution to line emission from stabilizing transitions for dielectronic recombination is found by finding the rate of radiationless capture assuming detailed balance with the rates of autoionization from a given ion.

### 2.3 Impact Excitation

The CROSS [22] suite of codes of Bar-Shalom, Klapisch and Oreg completes the version of the HULLAC package employed in the present work. CROSS uses RELAC's wavefunctions to compute the cross section for electron impact excitation from energy level $i$ to level $j$ of a given ion in the distorted wave approximation (DWA)

$$\sigma^{\mathrm{ex}}(i\rightarrow j) = \frac{2\pi a_0^2}{E_i g_i} \sum_J (2J+1) \sum_{\tilde{l}_i,\tilde{j}_i,\tilde{l}_j,\tilde{j}_j} \left| \langle \Gamma_j, J_j, \tilde{l}_j, \tilde{j}_j, J| \left[ \sum_{ij(i<j)}^{N+1} \frac{1}{r_{ij}} \right] |\Gamma_i, J_i, \tilde{l}_i, \tilde{j}_i, J\rangle \right|^2 , \qquad (9)$$

where $J_i$ and $J_j$ are the total angular momenta for the initial and final levels, respectively, $\Gamma_i$ and $\Gamma_j$ represent all other quantum numbers needed to specify the intermediate coupling initial and the final levels, respectively, $E_i$ is the incident electron energy in Rydbergs, $g_i$ is the statistical weight of the initial level, and $\tilde{l}_i$ and $\tilde{l}_j$ are the orbital angular momenta of the incident and scattered electrons, respectively, and $J$ is the total angular momentum of the target ion plus free-electron system. The two-electron Coulomb interaction operator is evaluated, in this case, between multiconfiguration states of the ion and a free, outgoing electron. The levels of all singly and doubly excited configurations have been allowed to mix with each target level; without precise spectroscopic comparisons (eg. Ref. [7, 8]) it is difficult to state whether this has a large effect on the spectra presented below. The DWA is a very good scheme for calculating the impact excitation rates between the levels of highly charged, high Z ions (that is, for all the cases considered here). The DWA misses resonance contributions to the excitation cross section ([23]); in certain cases, at low temperatures, resonance effects can contribute noticeably to the excitation cross section [24, 25, 26]. The fact that our collisional-radiative level population calculations (described below) include autoionization into excited levels of the final ion can (partially) account for this contribution [25]. It is felt that the DWA cross sections of the present calculations are highly accurate for the test cases considered. The final DWA rate coefficient for electron impact excitation between levels is found by averaging the electron impact excitation cross section over a Maxwellian distribution of free electron velocities

$$Q_{ij}^{\mathrm{ex}}(T_e) = \int_0^\infty v f(v) \sigma^{\mathrm{ex}}(i\rightarrow j) dv \qquad (10)$$

where $v$ is the electron velocity and $f(v)$ is the electron velocity distribution, a Gaussian integration technique is used.

## 3 b-b EMISSION

The level-to-level ionic transition rates above, including the autoionization rates from highly excited levels into all accessible levels of the next ion, as well as direct, impact ionization (DI), are used to

construct the collisional-radiative rate matrix

$$\frac{dn_j}{dt} = \sum_i n_i R_{i\to j} - n_j \sum_i R_{j\to i}, \tag{11}$$

where $n_j$ is the population in level $j$, and $R_{i\to j}$ is the total rate for transitions between level $i$ and $j$, possibly belonging to a neighboring iso-electronic sequence. The contribution of DI from both valence and innershell orbitals to the total ionization rate has been evaluated using the Lotz formula [27, 28] and a relativistic calculation of subshell binding energies [6]. The inverse of each ionization process, namely dielectronic recombination and three body recombination have been found according to the principle of detailed balance. Two methods have been employed to solve the system of equations in 11; both will be described in detail below. Briefly, for the set of test cases labeled 'version 1', the relative ion charge state densities for all charge states in the model have been found from an independent, off line calculation and then entered as constraints into equation 11; the populations for the excited levels in each ion were then found. This technique assumes the Quasi-Steady State (QSS) approximation in which the excited state populations equilibrate much faster than time scales for changes in the plasma conditions or in the ground state populations [29, 30, 31]. For the set of test cases labeled 'version 2', the relative populations in each level of each ion are found in the steady state, $\frac{dn_j}{dt} = 0$, by directly inverting the CR rate matrix. The resulting collisional-radiative line emission, $\varepsilon_{ij}$, for each transition from level $i$ to level $j$, is found (in photons cm$^3$ s$^{-1}$) at the specific transition energy, $h\nu_0$, for a given temperature and density,

$$\varepsilon_{ij}(h\nu_0) = n_i A_{ij}, \tag{12}$$

where $n_i$ is the (relative) population in the upper level and $A_{ij}$ is the radiative transition rate from level $i$ to level $j$. To produce a spectrum that can be compared to experiment the calculated line intensities are convolved with a Gaussian "instrument" profile, $\phi$, with a full width at half maximum (FWHM) equal to the resolution of the "spectrometer"

$$\varepsilon(h\nu) = \sum_{ij} \int_{\lambda_{min}}^{\lambda_{max}} \varepsilon_{ij}(h\nu_0)\phi(\lambda')d\lambda' \tag{13}$$

where the sum is over all transitions in the model. For the test cases Ar1, Ge1 and Ba1, a 1.0 eV FWHM has been used in equation 13, for the case of Au1, a 2.5 eV FWHM was used. The data for the present comparisons are found (in TW cm$^{-3}$ eV$^{-1}$ ) by multiplying the emissivity by the physical ion and electron densities

$$I_{bb}(h\nu) = n_{\rm ion} n_e \varepsilon(h\nu). \tag{14}$$

For the K-shell Ar1 test case treated here, singly and doubly excited configurations with $n \leq 8$, $l \leq 4$ have been considered. The doubly excited configurations are necessary to account for CI effects on the energies of some levels, and, more importantly for the present simulations, to allow for dielectronic recombination channels. For the Ar1 test case, I have considered 1053 fine-structure energy levels in the bare, H-, He- and Li-like argon ions. For the L-shell Ge1 test case, 5803 fine-structure energy levels in the F-like to Si-like ($Ge^{23+}$ to $Ge^{18+}$) ions have been considered ($5 \leq n^{\max} \leq 8$, $l \leq 4$). For the M-shell Ba1 test case, 7949 fine-structure energy levels in the Ni-like to Se-like ($Ba^{28+}$ to $Ba^{22+}$) ions have been considered ($n^{\max} \leq 6$). For Au1, I have considered only $n \leq 5$, $l \leq 4$ orbitals for the Co-like to Se-like ($Au^{52+}$ to $Au^{45+}$) ions. Explicit lists of eh configurations included in the calculation of each element's spectrum are given at the end of this document in tables 2 to 5. For the Ni-, Cu-, Zn- and Ga-like gold ions, $3d$ electrons are promoted to available $n$=4 and 5 orbitals with different perturbations of spectator $n$=4 electrons considered (the Ni-like ion had 2458 levels, Cu-like 2307 levels, Zn-like 3581 levels and Ga-like 3554 levels). This is different from the M-shell Ba1 case where only $n$=4 spectator electrons in the lowest energy orbitals were considered. The CR level population calculations were run on a COMPAQ AlphaServer 8400 with 6 GBytes of RAM; the f77 compiler was unable to handle a case with more than 8000 energy levels and more than $6\times10^6$ total (forward) transition rates. As a result, the Au1 case had to be treated in a manner different than

| Case | $< Z > \pm\sigma$ | | |
|---|---|---|---|
| | version 1 | version 2 | % difference |
| Ar1 | 17.899 ±0.059 | 17.931 ±0.036 | 0.18 |
| Ge1 | 20.949 ±0.378 | 22.894 ±0.057 | 10.28 |
| Ba1 | 25.792 ±0.666 | 27.198 ±0.214 | 5.45 |
| Au1 | 49.180 ±0.955 | – | – |

Table 1: Results for versions 1 and 2 of the cases considered.

the other three cases. Specific features in the resulting spectrum for each test case can be identified (see figures 1 to 7 below), including strong isolated lines and L- and M-shell transition arrays from individual ions. Specific features will not be called out or discussed further here.

For the Ar1, Ge1 and Ba1 test cases, two simulations of each have been computed. The first simulation in each case, version 1, has been computed in the QSS approximation, the relative ion densities are fixed according to an external ionization balance calculation, the level populations within a charge state are then found in equilibrium with their respective ground level. The external ionization balance calculation is done with the MCXSN module in the RIGEL code [32]. The code computes steady state non-LTE populations of screened hydrogenic configurations ($n \leq 8$) through a Monte Carlo calculation. In the calculation, a test ion samples the configuration space by undergoing radiative decays, collisional excitations and de-excitations, collisional and autoionizations, and dielectronic and three-body recombinations; the population of an ion species is equal to the fraction of time the test ion spends in the configurations of that species. The spectrum is then computed with the HULLAC atomic data for all ions in the MCXSN distribution whose fractional abundance is $\geq 0.005$ (0.5%). For the same cases, version 2 uses the same set of ions, with no assumptions about the relative ion fractions. The HULLAC-filled CR rate matrix is inverted directly to find the steady state ion populations. There are significant differences in the resulting average ion charge,

$$< Z >= \sum_{\text{ions}} f_q \times q \tag{15}$$

where $f_q$ is the fractional abundance of an ion with charge $q$, for the two versions of each case (see Table 1). The differences in the resulting $< Z >$ may be due to the full configuration space available for ionization and recombination events in the MCXSN calculations, including *all* ions for a given element and all singly, doubly, triply, etc. excited configurations within each ion. The steady-state CR calculations consistently produce a higher degree of ionization, which may be due to the limited configuration space available.

Due to limitations on the size of models that can be run, the case of Au1 is treated differently than either version 1 or version 2 of the calculations above. Each pair of gold ions is taken together, with the emphasis being on the autoionizing levels of the lower charge state; the calculated emission from the lower ion charge state in each case is weighed by the MCXSN calculation and summed to make the resulting Au1 spectrum. For the present work, the level of detail for Cu- to As-like Au ions is less than what has been previously considered [33]; thus, the absolute emissivity for the M-shell X-ray spectrum is probably underestimated. Version 1 of the Au1 test case is calculated with only the configurations explicitly listed in Table 5, version 3 of the Au1 test case has had a correction to the calculated Zn-like and Ga-like emissivities applied. In Ref. [33], it was explained that the total X-ray emissivity for some ion is proportional to the total population in "active" lower levels. In a separate calculation, all permutations of $4\ell$ electrons possible for the Zn-like and Ga-like ions have been considered; it is found that the population in the $n$=4 shell of the Zn-like ion is increased by 77% above that if only the configurations in Table 5 are considered. In like manner, if all permutations of the three $4\ell$ electrons are considered, the population in the $n$=4 shell of the Ga-like ion is enhanced by $\approx$ 44% above what is found including only the listed configurations in Table 5. These two enhancements have

been applied to the calculated emissivity for these two ions in Au1 version 3; the additional emission is not distributed spectrally in a physical way, and thus additional broadening of these ions' features due to the additional configurations is neglected. The final spectrum is nearly indistinguishable from that shown in Fig. 7 given the figure format, and it has not been plotted here.

# 4 f-b and f-f EMISSION

The free-bound (f-b) emission [34] (continuum emission from radiative recombination) for the present work is computed according to

$$\varepsilon^{fb}(h\nu) = \sum_{\text{ions}} f_q \varepsilon_q^{fb}(h\nu) \tag{16}$$

where $f_q$ is the fractional abundance of the ion with charge $q$ and $\varepsilon_q^{fb}(h\nu)$ is the thermal f-b emission coefficient for ion $q$. For photon energies $h\nu$ greater than threshold energies $\chi_i$ or $\frac{Z^2 Ry}{n^2}$ for ionization from the ground level or hydrogenic level with principal quantum number $n$, respectively, the thermal f-b emission coefficient is given by

$$\begin{aligned}\varepsilon_q^{fb}(h\nu) = \tfrac{2^5\pi e^6}{3mc^3}\left(\tfrac{2\pi}{3k_B m}\right)^{1/2} n_e n_{\text{ion}} \tfrac{q^2}{T_e^{1/2}} exp(-h\nu/k_B T_e)\Big[G_n \tfrac{\xi}{n^3}\tfrac{\chi_i}{k_B T_e} exp(\chi_i/k_B T_e) \\ + \textstyle\sum_{\nu'=n+1}^{n_{\max}} G_{\nu'} \tfrac{q^2 Ry}{\nu'^2 k_B T_e}\tfrac{2}{\nu'} exp(q^2 Ry/\nu'^2 k_B T_e)\Big]\end{aligned} \tag{17}$$

where $T_e$ is in Kelvin, $\chi_i$ is the ground level to ground level ionization energy from the recombined ion to the recombining ion, $\xi$ is the fraction of occupancy ($= 2n^2$) available for recombination in the lowest principal quantum shell of the initial ion, and $G_\nu$ is the appropriate Gaunt factor [35]. The first term in the brackets above is the contribution of recombination into the lowest available quantum shell, which may be partially occupied, the second term is recombination into all higher shells, which are assumed to be empty. The ground level to ground level ionization energies are computed from our atomic data using RELAC; the fraction of occupancy available for recombination is simply the number of holes in the lowest principal quantum shell of the initial ion, thus, for He-like ions, $\xi = 0$ in the $n$=1 shell, $\xi = 7/8$ for the $n$=2 shell in Li-like ions, etc. Hydrogenic energies are computed for the recombination into the higher quantum shells. Thermal Bremsstrahlung (f-f) emission for all photon energies is given by

$$\varepsilon^{ff}(h\nu) = \frac{2^5\pi e^6}{3mc^3}\left(\frac{2\pi}{3k_B m}\right)^{1/2} n_e n_{\text{ion}} \frac{Z^2}{T_e^{1/2}} exp(-h\nu/k_B T_e) g_{ff} \tag{18}$$

where $g_{ff}$ is the appropriate Gaunt factor and $Z$ is the average charge on all ions in the plasma. For f-b and f-f emission in units of TW cm$^{-3}$ eV$^{-1}$, the coefficient in front of equations 17 and 18 is given by

$$\frac{2^5\pi e^6}{3mc^3}\left(\frac{2\pi}{3k_B m}\right)^{1/2} = 1.64\times10^{-42} \tag{19}$$

with $n_e$ and $n_{\text{ion}}$ in cm$^{-3}$ and $T_e$ in Kelvin. The contributions of f-f and f-b emission to the computed spectra are obviously not the most sophisticated calculations possible; work is under way to improve the calculation of these quantities.

# References


[1] E. U. Condon and G. H. Shortley, *The Theory of Atomic Spectra* (Cambridge Univ. Press, London, 1935).

[2] A. Bar-Shalom, J. Oreg, W. H. Goldstein, D. Shvarts and A. Zigler, Phys. Rev. A **40**, 3183 (1989).

[3] A. Bar-Shalom and M. Klapisch, Computer Phys. Comm. **50**, 375 (1988).

[4] M. Klapisch, Computer Phys. Comm. **2**, 239 (1971).

[5] M. Aymar, M. Crance, and M. Klapisch, Journal de Physique C4 31, C4 (1970).

[6] M. Klapisch, J. Schwob, B. Fraenkel, and J. Oreg, J. Opt. Soc. Am. **67**, 148 (1977).

[7] J. E. Rice, K. B. Fournier, J. L. Terry, M. A. Graf, M. Finkenthal, E. S. Marmar and W. H. Goldstein, Phys. Rev. A **53**, 3953 (1996).

[8] J. E. Rice, K. B. Fournier, J. A. Goetz, E. S. Marmar and J. L. Terry, J. Phys. B: At. Mol. Opt. Phys. **33**, 5435 (2000).

[9] J. E. Rice, K. B. Fournier, M. A. Graf, J. L. Terry, M. Finkenthal, F. Bombarda, E. S. Marmar and W. H. Goldstein, Phys. Rev. A **51**, 3551 (1995).

[10] J. Bauche, C. Bauche-Arnoult, A. Bachelier, P. Palmeri, K. B. Fournier and W. H. Goldstein, J. Quant. Spect. Rad. Transfer **64**, 549 (2000).

[11] K. B. Fournier, W. H. Goldstein, M. May and M. Finkenthal, Phys. Rev. A **53**, 709 (1996).

[12] P. Mandelbaum, M. Finkenthal, J.-L. Schwob and M. Klapisch, Phys. Rev. A **35**, 5051 (1987).

[13] J. Bauche and C. Bauche-Arnoult, J. Phys. B: At. Mol. Phys. **20**, 1659 (1987).

[14] L. W. Fullerton and G. A. Rinker, Phys. Rev. A **13**, 1283 (1976).

[15] P. J. Mohr, Ann. of Physics **88**, 53 (1974).

[16] P. J. Mohr, Phys. Rev. Lett. **34**, 1050 (1975).

[17] P. J. Mohr, Phys. Rev. A **3**, 2338 (1982).

[18] G. W. Erickson, J. Phys. Chem. Ref. Data **6**, 831 (1977).

[19] I. P. Grant, J. Phys. B: At. Mol. Phys. **7**, 1458 (1974).

[20] E. Koenig, Physica **62**, 393 (1972), untranslated.

[21] J. Oreg, W. H. Goldstein, M. Klapisch, and A. Bar-Shalom, Phys. Rev. A **44**, 1750 (1991).

[22] A. Bar-Shalom, M. Klapisch, and J. Oreg, Phys. Rev. A **38**, 1773 (1988).

[23] P. G. Burke and W. D. Robb, Adv. At. Mol. Phys. **11**, 143 (1975).

[24] W. H. Goldstein, A. L. Osterheld, J. Oreg, A. Bar-Shalom, Ap. J. **344**, L37 (1989).

[25] K. B. Fournier, W. H. Goldstein, M. May, M. Finkenthal and J. L. Terry, Phys. Rev. A **53**, 3110 (1996).

[26] M. Mattioli, K. B. Fournier, L. Carraro, C. DeMichelis, P. Monier-Garbet, M. E. Puiatti, F. Sattin, P. Scarin and M. Valisa, Phys. Rev. E **60**, 4760 (1999).

[27] W. Lotz, Z. Phys. **216**, 241 (1968).

[28] W. Lotz, Z. Phys. **232**, 101 (1970).

[29] V. A. Boiko, I. Skobelev, A. Faenov, Sov. J. Plasma Phys. **10**, 82 (1984).

[30] D. Bates, A. Kingston, R. McWhirter, Proc. R. Soc. London **A267**, 297 (1962).

[31] D. Bates, A. Kingston, R. McWhirter, Proc. R. Soc. London **A270**, 155 (1962).

[32] B. G. Wilson, *et al.* in *Radiative Properties of Hot Dense Matter*, W. Goldstein, C. Hooper, J. Gauthier, J. Seely, R. W. Lee, editors (World Scientific, Singapore, 1991).

[33] K. B. Fournier, M. E. Foord, B. G. Wilson, S. H. Glenzer, K. L. Wong, R. S. Thoe, P. Beiersdorfer and P. T. Springer, in *Atomic Processes in Plasmas, Twelfth Topical Conference, AIP Conference Proceedings 547*, R. C. Mancini and R. A. Phaneuf, editors (AIP, Melville, NY, 2000).

[34] I. H. Hutchinson, *Principles of Plasma Diagnostics* (Cambridge Univ. Press, New York, NY, 1987).

[35] W. J. Karzas and R. Latter, Ap. J. Suppl. Series **6**, 167 (1961).

# 5 FIGURES

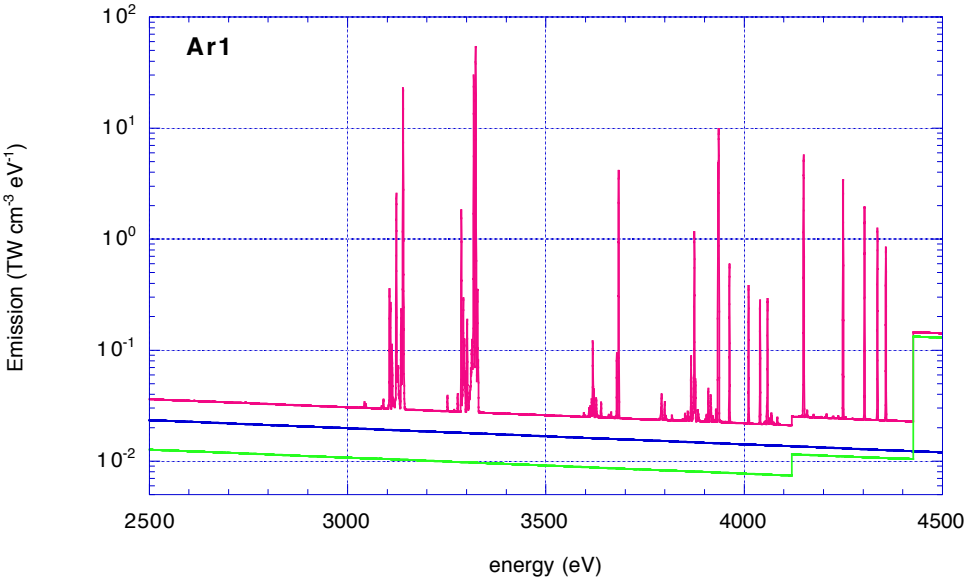


Figure 1: Case Ar1 with HULLAC atomic data and MCXSN ion state distribution (version 1), $T_e$ = 3.0 keV, $n_e = 3.0\times10^{21}$ cm$^{-3}$, $< Z > = 17.899\pm0.059$.

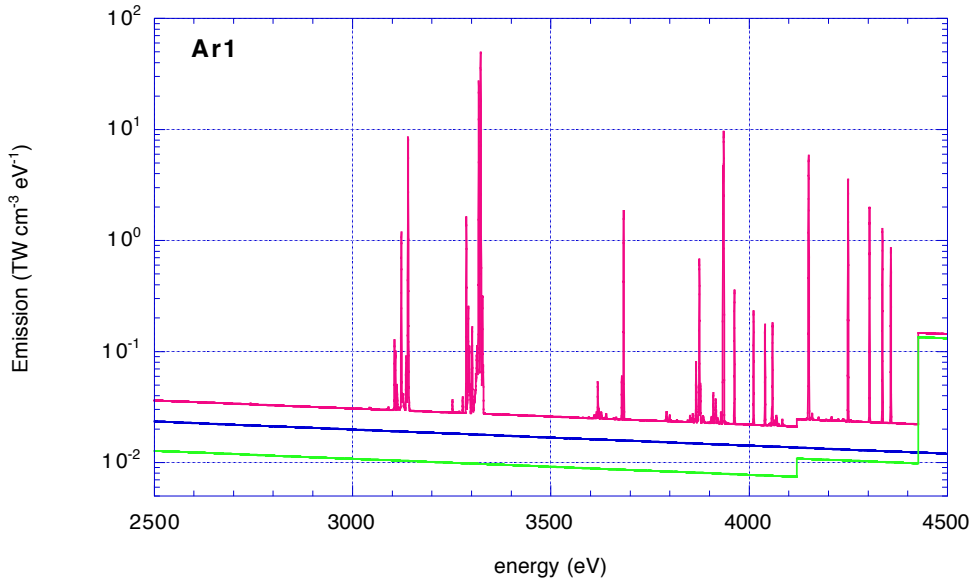


Figure 2: Case Ar1 with HULLAC atomic data and HULLAC ion state distribution (version 2), $T_e$ = 3.0 keV, $n_e = 3.0\times10^{21}$ cm$^{-3}$, $< Z > = 17.931\pm0.036$.

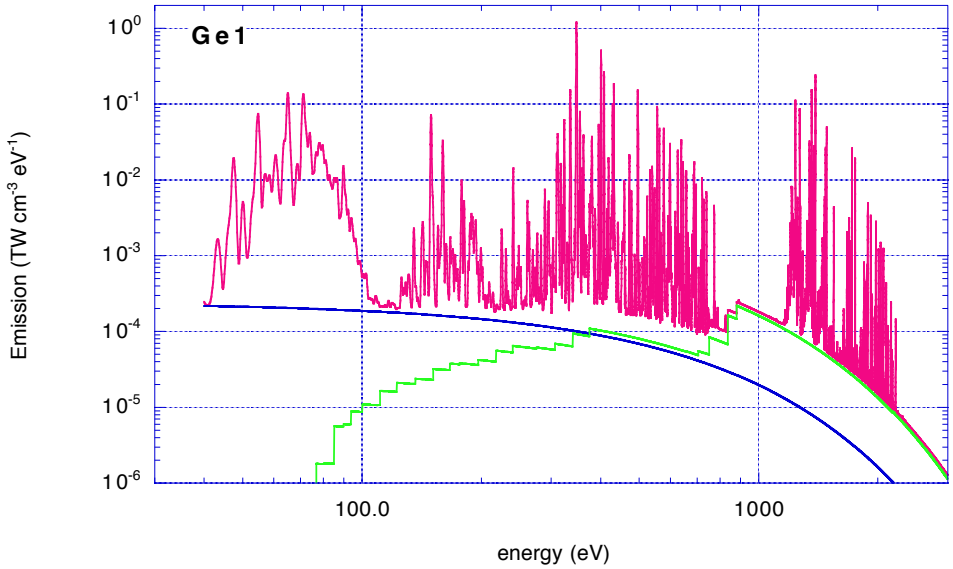


Figure 3: Case Ge1 with HULLAC atomic data and MCXSN ion state distribution (version 1), $T_e$ = 400 eV, $n_e = 1.0\times10^{20}$ cm$^{-3}$, $< Z > = 20.949\pm0.378$.

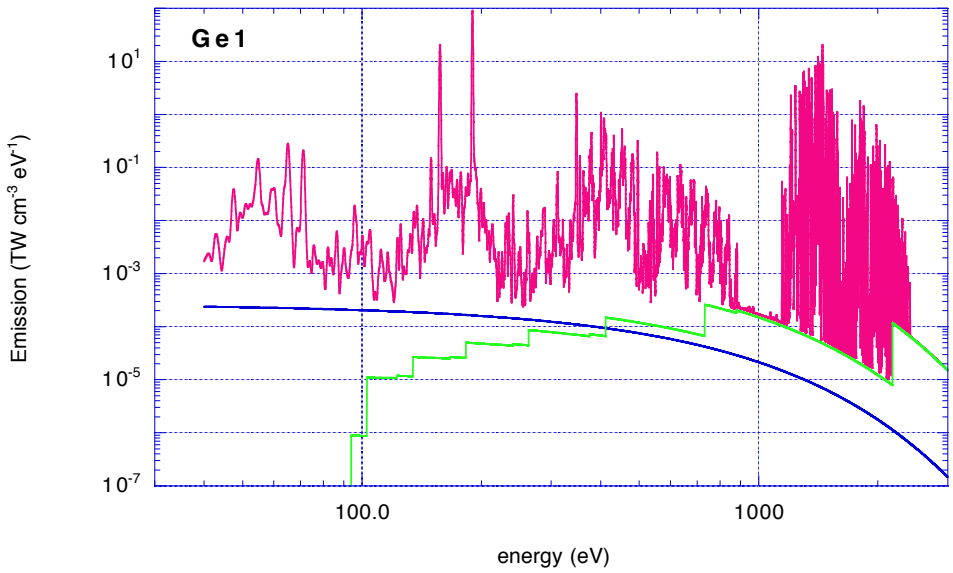


Figure 4: Case Ge1 with HULLAC atomic data and HULLAC ion state distribution (version 2), $T_e$ = 400 eV, $n_e = 1.0\times10^{20}$ cm$^{-3}$, $< Z > = 22.894\pm0.057$.

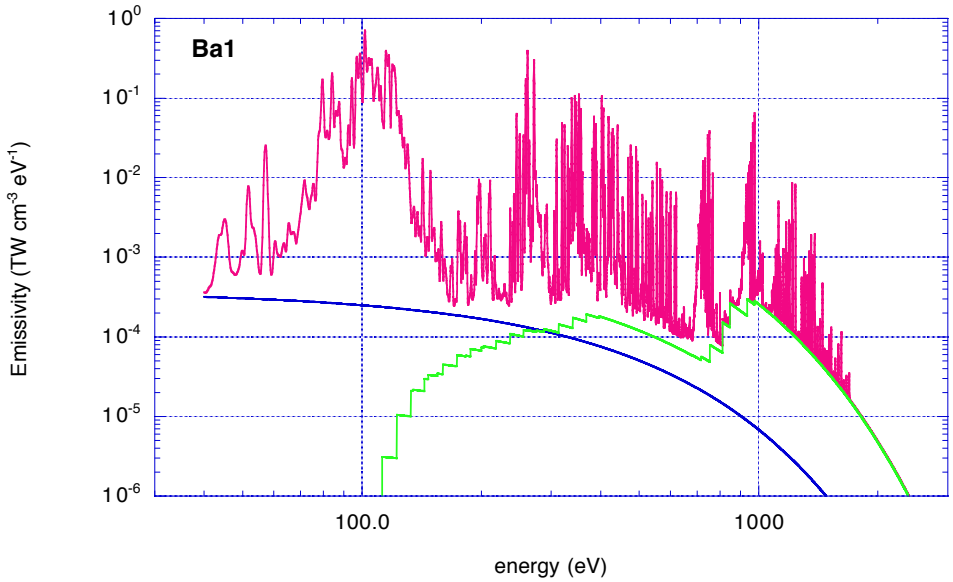


Figure 5: Case Ba1 with HULLAC atomic data and MCXSN ion state distribution (version 1), $T_e$ = 250 eV, $n_e = 1.0\times10^{20}$ cm$^{-3}$, $< Z > = 25.792\pm0.666$.

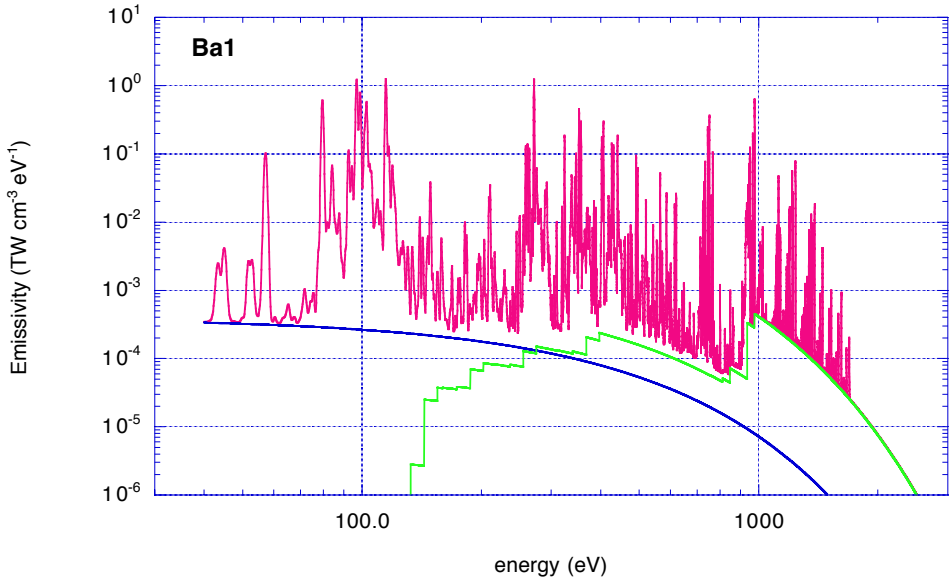


Figure 6: Case Ba1 with HULLAC atomic data and HULLAC ion state distribution (version 2), $T_e$ = 250 eV, $n_e = 1.0\times10^{20}$ cm$^{-3}$, $< Z > = 27.198\pm0.214$.

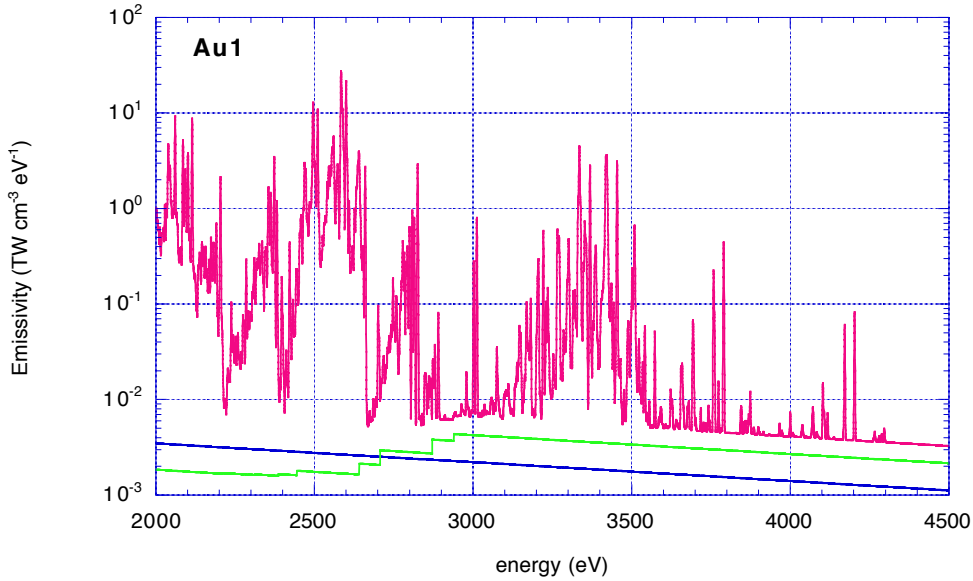


Figure 7: Case Au1 with HULLAC atomic data and MCXSN ion state distribution (version 1), $T_e$ = 2.2 keV, $n_e = 6.0\times10^{20}$ cm$^{-3}$, $< Z > = 49.180\pm0.955$.

# 6 CONFIGURATIONS CONSIDERED

Table 2: Configurations considered in computing Ar1 test spectrum

| configuration | |
|---|---|
| | H-like |
| $n\ell$ | $1 \leq n \leq 8$, $0 \leq \ell \leq 4$[a] |
| | He-like |
| $1sn\ell$ | $1 \leq n \leq 8$, $0 \leq \ell \leq 4$[b] |
| $2\ell n\ell'$ | $\ell$=0,1, $2 \leq n \leq 8$, $0 \leq \ell' \leq 3$[c] |
| $3\ell 3\ell'$ | $0 \leq \ell, \ell' \leq 2$ |
| | Li-like |
| $1s^2n\ell$ | $1 \leq n \leq 8$, $0 \leq \ell \leq 4$[b] |
| $1s2\ell n\ell'$ | $\ell$=0,1, $2 \leq n \leq 8$, $0 \leq \ell' \leq 3$[d] |
| $1s3\ell 3\ell'$ | $0 \leq \ell, \ell' \leq 2$ |

[a] $8f$ and $8g$ neglected
[b] $1s6g$, $1s(7f, g)$ and $1s(8f, g)$ neglected
[c] $2\ell 7f$ and $2\ell 8f$ neglected
[d] $1s2\ell 7f$ and $1s2\ell 8f$ neglected

Table 3: Configurations considered in computing Ge1 test spectrum

| configuration | |
|---|---|
| F-like | |
| $2s^2 2p^5$ | |
| $2s^2 2p^4 n\ell$ | $3 \leq n \leq 8$, $0 \leq \ell \leq 4$[a] |
| $2s2p^5 n\ell$ | $2 \leq n \leq 8$, $0 \leq \ell \leq 3$ |
| Ne-like | |
| $2s^2 2p^6$ | |
| $2s^2 2p^5 n\ell$ | $3 \leq n \leq 8$, $0 \leq \ell \leq 4$[b] |
| $2s^2 p^6 n\ell$ | $3 \leq n \leq 7$, $0 \leq \ell \leq 3$ |
| Na-like | |
| $2s^2 2p^6 n\ell$ | $3 \leq n \leq 8$, $0 \leq \ell \leq 4$[c] |
| $2s^2 2p^5 3sn\ell$ | $3 \leq n \leq 8$, $0 \leq \ell \leq 4$[d] |
| $2s2p^6 3sn\ell$ | $3 \leq n \leq 7$, $0 \leq \ell \leq 3$ |
| Mg-like | |
| $2s^2 2p^6 3\ell 3\ell'$ | $0 \leq \ell, \ell' \leq 2$ |
| $2s^2 2p^6 3sn\ell$ | $4 \leq n \leq 7$, $0 \leq \ell \leq 3$ |
| $2s^2 2p^5 3s^2 3\ell$ | $\ell = 1,2$ |
| $2s^2 2p^5 3s3p^2$ | |
| $2s^2 2p^5 3s^2 n\ell$ | $4 \leq n \leq 7$, $0 \leq \ell \leq 3$ |
| $2s^1 2p^6 3s^2 3\ell$ | $\ell = 1,2$ |
| $2s^1 2p^6 3s3p^2$ | |
| $2s^1 2p^6 3s^2 n\ell$ | $4 \leq n \leq 6$, $0 \leq \ell \leq 3$ |
| Al-like | |
| $2s^2 2p^6 3s^2 n\ell$ | $3 \leq n \leq 7$, $0 \leq \ell \leq 3$ |
| $2s^2 2p^6 3s3\ell 3\ell'$ | $1 \leq \ell, \ell' \leq 2$ |
| $2s^2 2p^5 3s^2 3pn\ell$ | $3 \leq n \leq 6$, $0 \leq \ell \leq 3$ |
| $2s^2 2p^5 3s3p^2 3\ell$ | $1 \leq \ell \leq 2$ |
| $2s^1 2p^6 3s^2 3pn\ell$ | $3 \leq n \leq 5$, $0 \leq \ell \leq 3$ |
| $2s^1 2p^6 3s3p^3$ | |
| Si-like | |
| $2s^2 2p^6 3s^2 3pn\ell$ | $3 \leq n \leq 5$, $0 \leq \ell \leq 3$ |
| $2s^2 2p^6 3s3p^3$ | |
| $2s^2 2p^6 3s3p^2 3d$ | |
| $2s^2 2p^6 3s3p3d^2$ | |
| $2s^2 2p^5 3s^2 3p^2 n\ell$ | $3 \leq n \leq 5$, $0 \leq \ell \leq 3$ |
| $2s^2 2p^5 3s3p^4$ | |
| $2s^2 2p^5 3s3p^3 3d$ | |
| $2s^1 2p^6 3s^2 3p^2 n\ell$ | $3 \leq n \leq 5$, $0 \leq \ell \leq 3$ |

[a] $2s^2 2p^4(6,7,8g)$ neglected
[b] $2s^2 2p^5(6,7,8g)$ neglected
[c] $2s^2 2p^6(6,7,8g)$ neglected
[d] $2s^2 2p^5 3s(6,7,8g)$ neglected

Table 4: Configurations considered in computing Ba1 test spectrum

| configuration | |
|---|---|
| | Ni-like |
| $3p^6 3d^{10}$ | |
| $3p^6 3d^9 n\ell$ | $4 \leq n \leq 6,\ 0 \leq \ell \leq 4$ |
| $3p^5 3d^{10} n\ell$ | $4 \leq n \leq 6,\ 0 \leq \ell \leq 4$ |
| | Cu-like |
| $3p^6 3d^{10} n\ell$ | $4 \leq n \leq 6,\ 0 \leq \ell \leq 4$ |
| $3p^6 3d^9 4sn\ell$ | $4 \leq n \leq 6,\ 0 \leq \ell \leq 4$ |
| $3p^5 3d^{10} 4sn\ell$ | $4 \leq n \leq 6,\ 0 \leq \ell \leq 4$ |
| | Zn-like |
| $3p^6 3d^{10} 4sn\ell$ | $4 \leq n \leq 6,\ 0 \leq \ell \leq 4$ |
| $3p^6 3d^9 4s^2 n\ell$ | $4 \leq n \leq 6,\ 0 \leq \ell \leq 4$ |
| $3p^5 3d^{10} 4s^2 n\ell$ | $4 \leq n \leq 6,\ 0 \leq \ell \leq 4$ |
| | Ga-like |
| $3p^6 3d^{10} 4s^2 n\ell$ | $4 \leq n \leq 6,\ 0 \leq \ell \leq 4$ |
| $3p^6 3d^{10} 4s4p4\ell$ | $1 \leq \ell \leq 3$ |
| $3p^6 3d^9 4s^2 4pn\ell$ | $4 \leq n \leq 6,\ 0 \leq \ell \leq 4$ |
| $3p^5 3d^{10} 4s^2 4pn\ell$ | $4 \leq n \leq 5,\ 0 \leq \ell \leq 3$ |
| | Ge-like |
| $3p^6 3d^{10} 4s^2 4p4\ell$ | $1 \leq \ell \leq 3$ |
| $3p^6 3d^{10} 4s4p^2 4\ell$ | $1 \leq \ell \leq 3$ |
| $3p^6 3d^9 4s^2 4p^2 n\ell$ | $4 \leq n \leq 5,\ 1 \leq \ell \leq 4$ |
| $3p^5 3d^{10} 4s^2 4p^2 4\ell$ | $1 \leq \ell \leq 3$ |
| | As-like |
| $3p^6 3d^{10} 4s^2 4p^2 4\ell$ | $1 \leq \ell \leq 3$ |
| $3p^6 3d^{10} 4s4p^3 4\ell$ | $1 \leq \ell \leq 3$ |
| $3p^6 3d^9 4s^2 4p^3 5\ell$ | $0 \leq \ell \leq 3$ |
| | Se-like |
| $3p^6 3d^{10} 4s^2 4p^3 4\ell$ | $1 \leq \ell \leq 3$ |
| $3p^6 3d^{10} 4s4p^4 4\ell$ | $1 \leq \ell \leq 3$ |
| $3p^6 3d^9 4s^2 4p^4 n\ell$ | $4 \leq n \leq 5,\ 1 \leq \ell \leq 3$ |
| $3p^5 3d^{10} 4s^2 4p^4 4\ell$ | $1 \leq \ell \leq 3$ |

Table 5: Configurations considered in computing Au1 test spectrum

| configuration | |
|---|---|
| | Co-like |
| $3s^2 3p^6 3d^9$ | |
| $3s^2 3p^5 3d^{10}$ | |
| $3s^1 3p^6 3d^{10}$ | |
| $3s^2 3p^6 3d^8 n\ell$ | $n$=4,5, $0 \leq \ell \leq 3$ |
| $3s^2 3p^5 3d^9 n\ell$ | $n$=4,5, $0 \leq \ell \leq 3$ |
| | Ni-like |
| $3s^2 3p^6 3d^{10}$ | |
| $3s^2 3p^6 3d^9 n\ell$ | $n$=4,5, $0 \leq \ell \leq 3$ |
| $3s^2 3p^5 3d^{10} n\ell$ | $n$=4,5, $0 \leq \ell \leq 3$ |
| $3s^2 3p^6 3d^8 4sn\ell$ | $n$=4,5, $\ell$=1,3 |
| $3s^2 3p^6 3d^8 4pn\ell$ | $n$=4,5, $\ell$=1,3 |
| $3s^2 3p^6 3d^8 4f^2$ | |
| | Cu-like |
| $3p^6 3d^{10} n\ell$ | $n$=4,5, $0 \leq \ell \leq 4$ |
| $3p^6 3d^9 4sn\ell$ | $n$=4,5, $0 \leq \ell \leq 4$ |
| $3p^6 3d^9 4\ell n\ell'$ | $1 \leq \ell \leq 3$, $n$=4,5, $0 \leq \ell' \leq 3$ |
| $3p^5 3d^{10} 4sn\ell$ | $n$=4,5, $0 \leq \ell \leq 4$ |
| | Zn-like |
| $3p^6 3d^{10} 4sn\ell$ | $4 \leq n \leq 5$, $0 \leq \ell \leq 4$ |
| $3p^6 3d^9 4s^2 n\ell$ | $4 \leq n \leq 5$, $0 \leq \ell \leq 4$ |
| $3p^5 3d^{10} 4s^2 n\ell$ | $4 \leq n \leq 5$, $0 \leq \ell \leq 4$ |
| $3p^6 3d^9 4s4\ell 4\ell'$ | $1 \leq \ell, \ell' \leq 3$ |
| $3p^6 3d^9 4s4\ell 5\ell'$ | $1 \leq \ell \leq 3$, $0 \leq \ell' \leq 3$[a] |
| | Ga-like |
| $3p^6 3d^{10} 4s^2 n\ell$ | $4 \leq n \leq 5$, $0 \leq \ell \leq 4$ |
| $3p^6 3d^{10} 4s4p4\ell$ | $1 \leq \ell \leq 3$ |
| $3p^6 3d^9 4s^2 4pn\ell$ | $4 \leq n \leq 5$, $0 \leq \ell \leq 4$ |
| $3p^5 3d^{10} 4s^2 4pn\ell$ | $4 \leq n \leq 5$, $0 \leq \ell \leq 3$ |
| $3p^5 3d^{10} 4s4p^2 n\ell$ | $n$=4,5, $0 \leq \ell \leq 3$ |

[a] $3p^6 3d^9 4s4f5s$ and $3p^6 3d^9 4s4f5d$ neglected

Table 5 continued

| | |
|---|---|
| | Ge-like |
| $3p^6 3d^{10} 4s^2 4p 4\ell$ | $1 \leq \ell \leq 3$ |
| $3p^6 3d^{10} 4s 4p^2 4\ell$ | $1 \leq \ell \leq 3$ |
| $3p^6 3d^9 4s^2 4p^2 n\ell$ | $4 \leq n \leq 5$, $1 \leq \ell \leq 4$ |
| $3p^5 3d^{10} 4s^2 4p^2 5\ell$ | $\ell$=0,2 |
| | As-like |
| $3p^6 3d^{10} 4s^2 4p^2 4\ell$ | $1 \leq \ell \leq 3$ |
| $3p^6 3d^{10} 4s 4p^3 4\ell$ | $1 \leq \ell \leq 3$ |
| $3p^6 3d^9 4s^2 4p^3 n\ell$ | $n$=4,5, $0 \leq \ell \leq 3$ |
| $3p^5 3d^{10} 4s^2 4p^3 nd$ | $n$=4,5 |
| | Se-like |
| $3p^6 3d^{10} 4s^2 4p^3 4\ell$ | $1 \leq \ell \leq 3$ |
| $3p^6 3d^{10} 4s 4p^4 4\ell$ | $1 \leq \ell \leq 3$ |
| $3p^6 3d^9 4s^2 4p^4 n\ell$ | $4 \leq n \leq 5$, $1 \leq \ell \leq 3$ |
| $3p^5 3d^{10} 4s^2 4p^4 4d$ | |
| $3p^5 3d^{10} 4s^2 4p^4 5\ell$ | $\ell$=s,d |